Thomas, F. B., Niitsu, A., Oregioni, A., Bartlett, G. J., & Woolfson, D. N. (2017). Conformational Dynamics of Asparagine at Coiled-Coil Interfaces. *Biochemistry*, *56*(50), 6544-6554. https://doi.org/10.1021/acs.biochem.7b00848

Conformational dynamics of asparagine at coiled-coil interfaces

Franziska Thomas[a,c‡*], Ai Niitsu[a‡], Alain Oregioni[d‡], Gail J. Bartlett[a‡], and Derek N. Woolfson[a,b,e*]

[a]School of Chemistry, University of Bristol, Cantock's Close, Bristol BS8 1TS, UK
[b]School of Biochemistry, University of Bristol, Medical Sciences Building, University Walk, Bristol BS8 1TD, UK
[c]Institute for Organic and Biomolecular Chemistry, Georg-August-Universität Göttingen, Tammannstr. 2, 37077 Göttingen, Germany
[d]MRC Biomedical NMR Centre, The Francis Crick Institute, 1 Midland Road, London NW1 1AT, UK
[e]BrisSynBio, University of Bristol, Life Sciences Building, Tyndall Avenue, Bristol BS8 1TQ, UK

KEYWORDS: asparagine, coiled coil, de novo protein design, protein dynamics, molecular dynamics simulations, protein NMR spectroscopy, structural bioinformatics.

ABSTRACT: Coiled coils (CCs) are among the best-understood protein folds. Nonetheless, there are gaps in our knowledge of CCs. Notably, CCs are likely to be structurally more dynamic than often considered. Here, we explore this in an abundant class of CCs, parallel dimers, focusing on polar asparagine (Asn) residues in the hydrophobic interface. It is well documented that such inclusions discriminate between different CC oligomers, which has been rationalized in terms of whether the Asn can make side-chain hydrogen bonds or not. Analysis of parallel CC dimers in the Protein Data Bank reveals a variety of Asn side-wchain conformations, but not all of these make the expected inter-side chain hydrogen bond. We probe the structure and dynamics of a *de novo* designed coiled-coil homodimer, CC-Di, by multidimensional NMR spectroscopy, including model-free dynamical analysis and relaxation-dispersion experiments. We find dynamic exchange on the millisecond timescale between Asn conformers with the side chains pointing into and out of the core. We perform molecular-dynamics (MD) simulations that are consistent with this, revealing that the side chains are highly dynamic, exchanging between hydrogen-bonded-paired conformations in picoseconds to nanoseconds. Combined, our data present a more-dynamic view for Asn at CC interfaces. Although inter-side chain hydrogen bonding states are the most abundant, Asn is not always buried or engaged in such interactions. Since interfacial Asn residues are key design features for modulating CC stability and recognition, these further insights into how they are accommodated within CC structures will aid their predictive modelling, engineering and design.

INTRODUCTION

Coiled coils (CCs) are one of the most abundant protein folds in nature.[1] They play key roles in many biological processes, directing and stabilizing protein structures and protein-protein interactions. Over the past three decades short CCs (20 – 40 amino acids long) have become favored models for studying protein folding and protein-protein interactions. As a result, CCs are one of the best understood protein-folding motifs available.[1,2] In turn, this has led to them being used widely in peptide and protein design and engineering, and for applications in materials science, biotechnology, synthetic biology and biomedicine.[1-4] Whilst sequence-to-structure relationships have been discerned, this does not mean that these are understood in physicochemico terms at the atomistic and molecular levels.

In CCs two or more α helices combine to form bundles with a left-handed supercoil. Underlying this is a regular seven-residue, or heptad-repeat sequence of hydrophobic (***h***) and polar (***p***) residues, ***hpphppp***, commonly denoted ***abcdefg***.[2,5] When configured into an α-helix this pattern brings together the ***a*** and ***d*** positions. The resulting hydrophobic face drives association of multiple helices to form the bundles. These helix-helix interfaces are cemented by intimate side-chain interactions termed knobs-into-holes (KIH) packing.[6]

Despite this apparent simplicity, CCs show a diversity of oligomeric states, the helices can be parallel or antiparallel, and the complexes can be ho-

mo- or heteromeric. In nature, CCs are mostly dimeric, trimeric and tetrameric, although pentamers and higher-order oligomers are known both in nature and through design.[2,5,7] The influence of the type of the residues at the ***a*** and ***d*** positions on the oligomeric state has been studied systematically in the GCN4 leucine-zipper peptide (GCN4-p1).[8] In detail, isoleucine (Ile) at ***a*** plus leucine (Leu) at ***d*** positions guide association to parallel CC dimers; having Ile at both ***a*** and ***d*** results in trimers; and Leu at ***a*** plus Ile at ***d*** are characteristic of tetrameric assemblies.

Charged amino acids at the ***e*** and ***g*** positions, notably glutamic acid (Glu) and lysine (Lys), also play roles in CC structure and stability. These residues can direct CC folding, parallel or antiparallel helix orientation, and homo- versus heterotypic assembly.[9-14]

Despite the importance of ***hp*** patterns, polar residues occur surprisingly frequently at ***a*** and ***d***, accounting for ≈25% of all residues in the CC+ database of CCs culled from the Protein Data Bank (PDB).[15,16] Although thermodynamically destabilizing, it has become evident that these residues play important roles in the specification of CC oligomeric state and orientation.[10,13,17-21] Indeed, such residues are often highly conserved through evolution.[22]

Asparagine (Asn) is amongst the most abundant of these polar inclusions.[23] For example, in the trimeric CC domains of the autotransporter adhesins conserved Asn residues occur at ***d***.[24] X-ray crystal structures of these motifs show that these side chains are often associated with sequestered halide anions in the core. More commonly, however, buried Asn residues occur at the ***a*** sites of CC dimers, for example the bZip transcription factors,[25,26] where the residues is often required for dimer specificity.[8,27,28] Indeed, Asn-at-***a*** is now almost an obligatory design feature in the specification of completely *de novo* designed of homo- and heterodimeric CCs, and in the construction of orthogonal CC pairs.[13,17,29-31] However, as a cautionary note and additional nuance to this, the Asn-at-***a*** has to be located centrally to specify oligomer state otherwise alternative and unintended CC assemblies can be observed.[32]

These sequence-to-structure relationships present rules for the *de novo* design of CCs. On this basis, we and others have designed and characterized sets of homomeric and heteromeric coiled coils, which have been used in synthetic biology and materials design.[12,13,17,33] However, the demands on *de novo* CCs through these and advancing applications are increasing; notably, larger sets of orthogonal heterodimers are required for more-complex CC assemblies,[34,35] and structures beyond simple dimers to tetramers are being designed.[7,36] As a consequence, more sequence-to-structure relationships are needed, and we need a deeper understanding of those that we have.

An important aspect of this will be to understand the dynamics of CCs, especially of residues at the CC interfaces, and how these contribute to CC specification. Analyses of crystal structures alone will not be sufficient as these give only one or a small number of the many possible CC conformations. The controversial discussion of whether interhelical electrostatic interactions in CC dimers are stabilizing or not provides an example of this: Whilst X-ray crystal structures anticipate salt-bridge formation at CC interfaces, solution-phase nuclear magnetic resonance (NMR) gives a more-complex view and generally identify fewer salt bridges than expected.[37-41] In GCN4-p1, acidic residues in these pairs make little contribution to dimer stability, but certain basic residues do contribute favorably.[42,43] Nonetheless, pH titrations removing any formal electrostatic interactions result in subtle changes in the overall CC structure and supercoil.[44]

For buried Asn residues: hydrogen bonding between the amide side chains is observed in X-ray crystal structures,[25] and is commonly assumed to offset the destabilization of burying these functional groups. As with salt-bridge interactions, however, these interactions are not straightforward, and are more likely highly dynamic. Indeed, the aforementioned pH titration of GCN4-p1 reveals a range of Asn side-chain conformations.[44] Related to this, the native dimeric state of GCN4-p1, which has a central Asn-at-***a***, forms trimers under certain conditions.[45] In this state, the Asn side chains point out from the hydrophobic core and water fills the space left behind. This dimer-trimer ambiguity is accentuated by mutating Asn→Gln in GCN4 system.[28] These conformational dynamics in GCN4-p1 might be extreme, but they are not unique. NMR spectroscopy focusing on core Asn residues of a disulfide-linked Jun homodimer confirms hydrogen bonded Asn side chains, but suggests fast exchange between two different asymmetric hydrogen bonds.[46]

Due to the importance of the buried Asn residues in CC assembly, recognition and design, it is imperative to completely understand the dynamics and interactions of these inclusions. This would provide clarity on the mechanism of dimer specification by Asn in CC dimers, and facilitate the manipu-

lation of these interactions to redesign and design CC interfaces.

Here we shed light on Asn inclusions through detailed analysis, experiments and modelling of a *de novo* designed parallel CC homodimer, CC-Di.[17] CC-Di has four heptads with Asn at the ***a*** site of the third. This is highly specifying for dimer, as mutation to the canonical Ile gives a trimer.[17] The X-ray crystal structure of the dimer shows that the core Asn residues are dynamic with multiple Asn-Asn paired conformations present. We combine analyses of Asn residues buried in dimeric CC interfaces of the PDB and 2D - 4D NMR experiments to probe the dynamics Asn-Asn interaction directly. These reveal multiple paired Asn-Asn conformations. Whilst the major conformers are the hydrogen-bonded pairs, other states exist in which the Asn side chains point out from the hydrophobic core and do not interact with each other. Finally, we perform molecular dynamics (MD) studies to visualize a mechanism for this exchange process.

MATERIALS AND METHODS

General. Fmoc-protected amino acids, HBTU and peptide grade DMF were purchased from AGTC Bioproducts (Hessle, U.K.). H-Rink Amide-Chemmatrix® resin was acquired from PCAS BioMatrix Inc. (Saint-Jean-sur-Richelieu, Canada). 15N labelled amino acids Fmoc-Asn(Trt)-OH and Fmoc-Leu-OH were obtained from Sigma-Aldrich. H-Leu-OH, which was 13C labelled at the α-carbon was acquired from Campro Scientific (Berlin, Germany) and subsequently Fmoc-protected following standard procedures. All other chemicals were purchased form Fisher Scientific (Loughborough, U.K.). Water was purified with a Synergy® UV water purification system from Millipore. Peptide concentrations were determined by UV-absorbance (λ280 (Trp) = 5690 mol–1 cm–1, λ280 (Tyr) = 1280 mol–1 cm–1) using a NanoDrop 2000 Spectrophotometer from Thermo Scientific.

Peptide Synthesis. The peptide amides were synthesized on a H-Rink Amide-Chemmatrix® resin on a 0.1 mmol scale on a CEM microwave-assisted synthesizer. The synthesis was conducted via a standard Fmoc-protocol using DIC/HOBt as coupling reagent mixture. N-acetylation of the peptides was carried out by using acetic acid anhydride / pyridine (1:9). Acidic cleavage from the resin was achieved by a treatment of the resin with a mixture of trifluoroacetic acid (TFA) / triisopropylsilane / water (90:5:5, 3 h). The resin was extracted with additional TFA (5 mL), and the combined extracts were concentrated to a third of the initial volume under a flow of nitrogen. The crude peptide was then precipitated in cold diethylether (40 mL) and isolated by centrifugation and decantation of the ether. The precipitate was redissolved in 5 mL of a 1:1 mixture of acetonitrile and water and then freeze-dried to give a fine white solid.

Peptide purification. Peptides were purified by reverse-phase HPLC using a JASCO chromatography system and a Kromatek C18HQsil column (150 by 10 mm) using a linear gradient of water and acetonitrile (buffer A: water, 0.1 % TFA, buffer B: acetonitrile, 0.1 % TFA) run from 30-60 % buffer B over 30 min.

Peptide characterization. The peptides were characterized by mass spectrometry on a Bruker Daltonics UltrafleXtreme MALDI-TOF mass spectrometer operating in positive-ion reflector mode (matrix: α-cyano-4-hydroxycinnamic acid (CHCA), external calibration). High-resolution mass spectrometry was performed on a Waters Synapt G2-S nano-ESI-IMS-TOF mass spectrometer. Analytical HPLC measurements were performed using a JASCO chromatography system and a Phenomenex® Prodigy ODS-3 (5 μm, 4.6 x 100 mm). For peptide characterization a linear gradient of water and acetonitrile (buffer A: water, 0.1 % TFA, buffer B: acetonitrile, 0.1 % TFA) run from 20-80 % over 20 min was used. Chromatograms were monitored at 220 and 280 nm wavelengths.

NMR Measurements. The unlabelled and labelled CC-Di samples were made at 2 mM total peptide concentration in a phosphate buffer (8.2 mM sodium phosphate, 1.8 mM potassium phosphate, 68 mM sodium chloride, 1.4 mM potassium chloride, pH adjusted to 7.0), containing 10% D_2O at 20°C or 40°C. The NMR data were acquired on Bruker Avance and Avance III spectrometers at 600 MHz (TCI Cryoprobe) and Bruker Avance III HD spectrometers at 700 MHz (QCI Cryoprobe) and 800 MHz (TCI Cryoprobe). Primary assignments and structure calculations for CC-Di were obtained from the unlabelled sample using proton 2D TOCSY (60ms mixing time), 2D NOESY (80 ms and 150 ms mixing time), 2D COSY and ^{15}N-edited SOFAST-HMQC[47] at 600 MHz.

A selectively labelled ^{15}N Leu and Asn sample was used at 600 MHz and 700 MHz to study the dynamic properties of CC-Di. A model free approach was used on the data from ^{15}N-edited- T1, -T2 and ^{15}N ^{1}NOE of the backbone residues.[48] The conformational exchange detected on the labelled Asn amide side-chains was studied by ^{15}N-edited relaxation dispersion experiments.[49]

To study the connectivity of CC-Di, an equimolar mixture of 1mM selectively ^{15}NNε-labelled-Asn17 sample and 1 mM selectively ^{13}Cα -labelled on Leu13 sample was prepared, yielding a 0.5 mM abundance of CC-Di with one coil being ^{15}N-labelled-Asn and the other ^{13}C-labelled-Leu. The trans-coil connectivity was checked through a 4D ^{13}C-edited-HSQC-NOE-^{15}N-edited-HMQC[50] with 120 ms NOESY mixing time at 800 MHz. Due to the selective labelling limiting the number of peaks observed, only the proton-proton 2D plane was necessary.

The same sequence was used in a 1D form to record an NOE build-up to gain insight into the cross-relaxation of the labelled spins. The NOE build-up rate is proportional to the cross-relaxation σ from a spin S to a spin I, following:

$$\frac{dI}{dt} = \sigma_{IS} S_{Z0} \qquad (1)$$

with S_{z0} being the starting magnetisation of spin *S*.

In turn, the cross relaxation is linked to the distance R_{IS} between the spin I and S:[51]

$$R_{IS} = \left(\frac{59.94\tau_C}{\sigma_{IS}}\right)^{1/6} \quad (2)$$

with τ_C being the molecular correlation time in ns giving R_{IS} in Å.

One problem with measuring the cross-relaxation is a lack of normalisation of the NMR signals. Here, we use the knowledge of the $N17_{NH}$-$L13_{C\alpha H}$ protons distance from the crystal structure: $R^X_{N17\text{-}L13}$. From the equation *(2)* above we get:

$$\sigma_{NH} = \frac{59.94\tau_C}{(R^X_{N17-L13})^6} \quad (3)$$

where σ_{NH} is the cross-relaxation between the N17 amide proton of one strand and the L13 alpha proton of the other strand of the dimer and τ_C the global correlation time of the dimer. Replacing sigma in equation *(1)* gives the opportunity to get rid of S_{z0} (representing the L13Hα starting magnetisation):

$$S_{Z0} = \frac{dI_{NH}}{dt}\frac{(R^X_{N17-L13})^6}{59.94\tau_C} \quad (4)$$

with dI_{NH}/dt being the NOE build-up curve of the N17 amide proton. Since the starting point of the magnetisation for the NOE transfer to the side-chains of N17 was also L13Hα, we can substitute S_{z0} in the build-up calculations, giving a way to evaluate the cross-relaxation and hence the distances to the side-chains:

$$\sigma_{SC} = \frac{\frac{dI_{SC}}{dt}}{\frac{dI_{NH}}{dt}}\frac{59.94\tau_C}{(R^X_{N17-L13})^6} \quad (5)$$

with σ_{SC} is the cross-relaxation between the N17 side-chain protons of one strand and the L13 α proton of the other strand and τ_C the global correlation time of the dimer. The ratio of the build-up curves can be substituted for the ratio of the slopes of the build-up curves calculated with a normalisation to the NH peaks. This allows for a distance to be calculated once put back into equation *(2)*:

$$R_{SC} = R^X_{N17-L13} \cdot \left(\frac{\frac{dI_{NH}}{dt}}{\frac{dI_{SC}}{dt}}\right)^{1/6} \quad (6)$$

The equations *(1-6)* are set for a standard set-up of proton-proton interaction. In our case, we know that the side-chains are in exchange. However, since the exchange rate is slow/intermediate (only one peak is seen) and likely to be around 20 s^{-1}, hence substantially more than the R1 values of any backbone or side-chain residues, the exchange dependence on the measured (R1, NOE build-up) or calculated (σ_{IS} or R_{IS}) values are averaged but also unique, and the equations above still stand. Furthermore, since the exchange is slower than the overall molecular tumbling, the averaging is truly over $\langle r^{-6}\rangle$, and not $\langle r^{-3}\rangle$.[52] The distances and build-up slopes calculated from equations *(1-6)* are shown in Table S3.

The build-up curves were calculated with a linear regression model and the errors with an error propagation model using R (R Core Team (2016). R: A language and environment for statistical computing (https://www.R-project.org/).

The NMR data was processed with either NMRPipe[53] or Bruker Tospsin and MestreNova. Structural data were analysed with Bruker Topspin or MestreNova and dynamic data were analysed with RELAX NMR.[54]

Molecular Dynamics Simulations. Starting PDB structures of dimeric assemblies with asparagine-at-a and asparagine-at-d derived from PDB 4DZM were capped at the N-terminus with an acetyl residue and at the C-terminus with an amide residue. These were converted to GROMACS co-ordinate and topology files using the AMBER99sb-ildn forcefield, and solvated in a dodecahedral box 1.5 nm larger than the peptide assembly in all directions with TIP3P water molecules. To simulate isotonic ion concentrations the genion utility in GROMACS was used to add Na^+ and Cl^- ions to a final ionic strength of 150 mM at neutral pH with no overall charge. Structures were subjected to an initial 200-step energy minimization using the steepest descents method. Simulations were performed using periodic boundary conditions. Short range electrostatic and van der Waals' interactions were truncated at 1.4 nm, while long-range electrostatics were treated with the particle-mesh Ewald's method, and a long-range dispersion correction was applied. Pressure was controlled by Berendsen's thermostat and temperature by the V-rescale thermostat. Simulations were integrated with a leap-frog algorithm over a 2 fs timestep, constraining bond vibrations with the P-LINCS method. For replica exchange, 64 replicas were created with exponentially distributed temperatures from 298 K – 419 K. These were subjected to an additional 200-step energy minimization as before, followed by 200 ps of position-restrained MD in which the peptide atom coordinates were fixed. An initial 200 ps unrestrained REMD run showed average exchange rates for both simulations ranging from 0.2-0.3, this was judged sufficient for a longer REMD simulation runs of 100 ns, giving a total REMD simulation time of 6.4 μs for each system. Simulations were performed using 64 nodes on the Bristol High Performance Computer BlueCrystal.[55] In order to test for convergence of the system, the distributions of rms-distance for each structure in each replica were compared and found to be equivalent (Figure S9).

Replica trajectories were concatenated such that each trajectory had a continuous temperature, and the replica with the temperature closest to that at which the NMR experiments were performed (313K) was selected for analysis.

RESULTS

Multiple asparagine conformers occur in coiled-coil interfaces. The X-ray crystal structure of the *de novo* designed parallel homodimeric CC, CC-Di (PDB identifier 4DZM, Table S1), reveals a near-C2-

symmetric quaternary assembly.[17] However, the crystallographic unit cell contains two peptide monomers from different assemblies, and C2 symmetry is broken by the Asn residues at position 17, which populate three primary side-chain dihedrals (χ_1). (*n.b.* As detailed below, the full description of the side-chain conformation requires this plus the second dihedral angle (χ_2), but for the immediate discussion, we only need to consider χ_1 as this directs the side chain relative to the interface.) We refer to the three conformers as '*inside*' ($\chi_1 \approx$ -70°, "***g***$^-$"), '*middle*' ($\chi_1 \approx \pm$180°, "***t***"), and '*out*' ($\chi_1 \approx$ -120°, "***t****") (Fig. 1A). As a result, there are nine potential paired conformations for the Asn-Asn pair. Two of these could result in hydrogen bonding between the side chains (both 'inside-middle' conformations) if the second dihedral allowed; in six, the residues are too distant to form hydrogen bonds (the two 'inside-out', 'middle-middle', two 'middle-out', and 'out-out' conformations); and there is one disallowed conformation ('inside-inside') as the Asn side chains would clash in full quaternary models.

To test if this heterogeneity of Asn-Asn interactions was representative of Asn-containing CC dimers more generally, we inspected such structures in the RCSB Protein Data Bank (PDB).[15] We used CC+[16] to mine the PDB for parallel CC dimers containing pairs of Asn residues at ***a*** positions. The conformations of the Asn side chains varied (Fig. 1B). However, clustering the structures according to both side-chain dihedral angles, χ_1 and χ_2 referred to above, revealed a number of specific conformations (Fig. 1C). The most-populated conformer was the 'inside-middle' arrangement, more formally ***g***$^-$***o***/***tg***$^-$,[56] with approximately two thirds of structures accounting for this state (Fig. 1C(i)). This promotes a buried hydrogen bond between the two Asn side chains. Of the other, less-populated conformations, only one allows a hydrogen bond (Fig. 1C(ii), ***tg***$^+$/***g***$^-$***t***), which is an alternative configuration within the '*inside-middle*' group, equivalent to ***g***$^-$***o***/***tg***$^-$ but with the amide atoms swapped. The rest either preclude a hydrogen bond altogether (Fig. 1C(v) and 1C(vi)), or allow a hydrogen bond only if the side chain of one Asn residue were to flip at the Cγ position (Fig. 1C(iii) and 1C(iv)). *N.b.,* This analysis assumes that the atoms have been built into these structures correctly, and given the nature of the Asn side chain there could be some ambiguity in the placement of atoms.

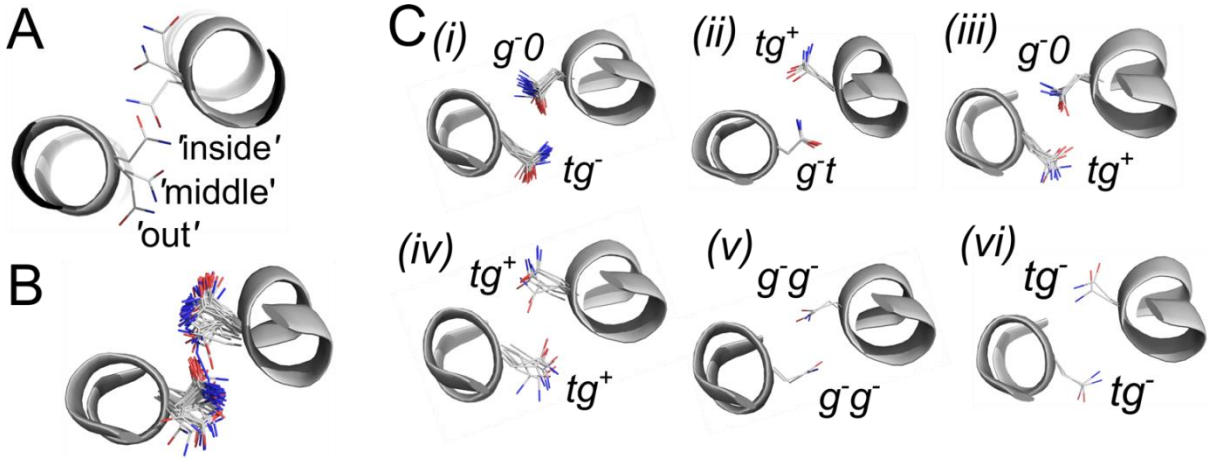

Figure 1. Conformations adopted by Asn pairs in dimeric CC interfaces of the PDB. Structures were superposed on the backbone atoms using ProFit.[57] Images generated using PyMOL (www.pymol.org). (A) Multiple conformations of asparagine residues in PDB entry 4DZM. Two of the nine potential conformations allow hydrogen-bonding between the Asn residues, one would be prohibited due to steric clashes and others would point both residues out into solvent. (B) All Asn at ***a*** pairs identified from CC+ using a redundancy cut-off of 70%. (C) Structures grouped according to side-chain dihedral combinations. Side-chain dihedrals χ_1 and χ_2 were calculated using a Python script. χ_1 is the dihedral formed by atoms N,C_α,C_β,C_γ and χ_2 is the dihedral formed by atoms C_α,C_β,C_γ,$O_{\delta 1}$. These were classified as follows: *t*, $\chi > 120°$ or $\chi < -120°$, with *t** assigned a subclass of *t* where $\chi \approx$ +/- 120°; g^-, $\chi < 0°$ and $\chi > -120°$; g^+, $\chi > 0°$ and $\chi < 120°$. 'o' indicates a dihedral angle with a mean of around 0° which classifies as neither g^- nor g^+. (i), 47 examples; (ii), 4 examples; (iii), 7 examples; (iv), 7 examples; (v), 2 examples; (vi), 2 examples. A further three combinations of side-chain dihedral angles had one example each and are not depicted: g^+g^+/g^-g^+, g^+g^-/tg^+ and g^-g^+/g^+g^+.

As with CC-Di, we found several of the structures in the broader PDB with Asn in multiple conformations. One was in a CC from *M. tuberculosis* in which 3 conformers of the Asn are seen on each strand (PDB identifier 3m91,[58]). This structure is complicated further by two flanking helices that

provide additional Asn residues that compete for hydrogen bonding with the central Asn side chains (Fig. S1). Interestingly and more generally, such potential interactions between Asn residues often only became apparent when symmetry mates were generated, and not all the combinations of conformations listed in the PDB file would be allowed due to steric clashing (Fig. 1A).

It is clear from this analysis that there are multiple possible individual and paired conformations for buried Asn residues at dimeric CC interfaces, which opens possibilities for dynamics between these.

The interfacial asparagine of CC-Di is dynamic but forms hydrogen bonds. We turned to NMR spectroscopy of CC-Di in solution to probe side-chain dynamics experimentally (Table S1, Fig. S2). ^{1}H chemical shifts for CC-Di were assigned using 2D ^{1}H-^{1}H correlation spectra (TOCSY and NOESY, Table S2). This gave a single set of resonances consistent with the largely C2 symmetric X-ray structure. We extracted structural information for CC-Di from the intramolecular connectivities observed in the 2D NOESY, Fig. 2A. *$d_{N,N}(i, i+1)$, $d_{\alpha,N}(i, i+3)$ and $d_{\alpha,N}(i, i+4)$* NOEs were found along the whole peptide sequence, indicative of a fully α-helical structure. This was corroborated by negative differences in chemical shifts (Δδ values) of the αH protons from those expected for the fully unfolded peptide (Fig. 2B).

More specifically, we found that the Asn resonances were broadened in all NMR spectra (Fig. 2Ci-iii), and that this was most apparent for the side-chain resonances (Fig. 2Ciii). This could be due in part to hydrogen bonding or even exchange with solvent. However, the cross-peak between the side-chain amide protons (Asn17(HD21-HD22)) was broad and asymmetric indicative of multiple resonances and an ensemble of conformers (Fig. 2Ciii). Consequently, the resulting weaker signal meant that Asn side-chain resonances were not detected in 2D ^{1}H-^{15}N correlation spectra (^{15}N-edited SOFAST-HMQC and ^{1}H-^{15}N HSQC, Fig. S6B).

To resolve these issues, we introduced site-specific isotopic labelling. First, CC-Di was made with Asn17 ^{15}N-labelled (CC-Di$_{N}$(Asn), Table S1, Fig. S3). This gave visible Asn17(HD) resonances in the 2D ^{1}H-^{15}N correlation spectrum at 20°C. Peak broadening was observed for both resonances, but to different extents (Fig. S6C): the 17Asn(HD22) resonance was significantly lowered in intensity compared with 17Asn-HD21. On this basis, we posit that HD22 is likely involved in hydrogen bonding, and, based on our analysis of the PDB, that this hydrogen bond is formed between the Asn residues of partnering CC strands.

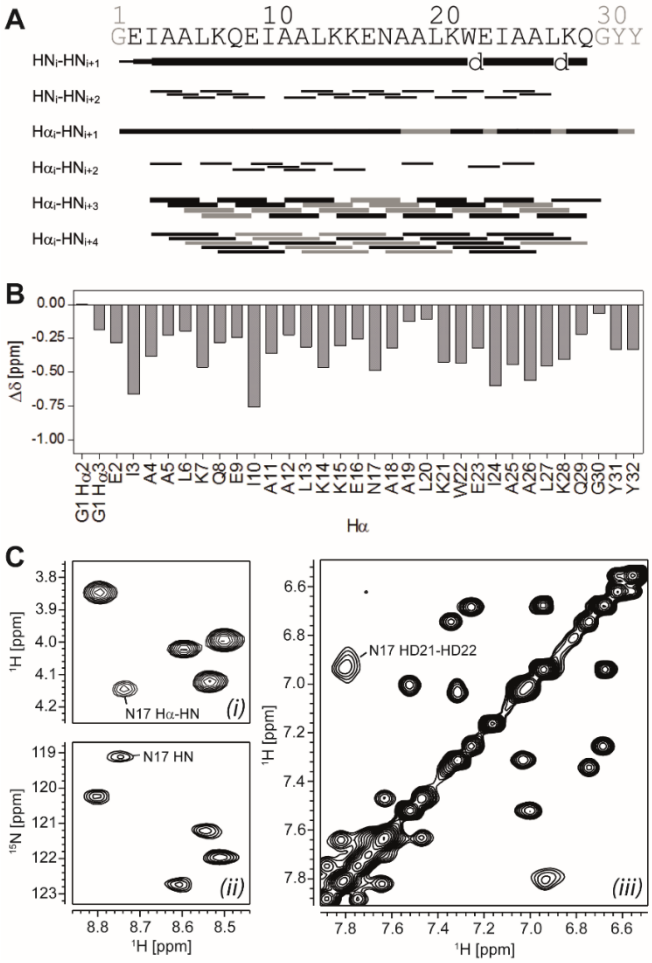

Figure 2. Structural elucidation of CC-Di in solution by NMR spectroscopy. (A) NOE connectivity table based on TOCSY and NOESY experiments for CC-Di measured at 20 °C. (B) Δδ of the Hα proton chemical shifts. Δδ values were calculated as the difference in the observed chemical shifts and the sequence-corrected random-coil chemical shifts.[59] (C) TOCSY (i), ^{15}N-edited SOFAST-HMQC (ii), and NOESY (iii) spectra showing signal broadening of the N17 amide backbone resonances (i & ii) and the amide side-chain resonances (iii). Conditions: 2 mM total peptide concentration, 10 mM phosphate buffer (68 mM sodium chloride, 1.4 mM potassium chloride, pH adjusted to 7.0), 10% D_2O, using a cryoprobe-equipped Bruker 600 MHz spectrometer.

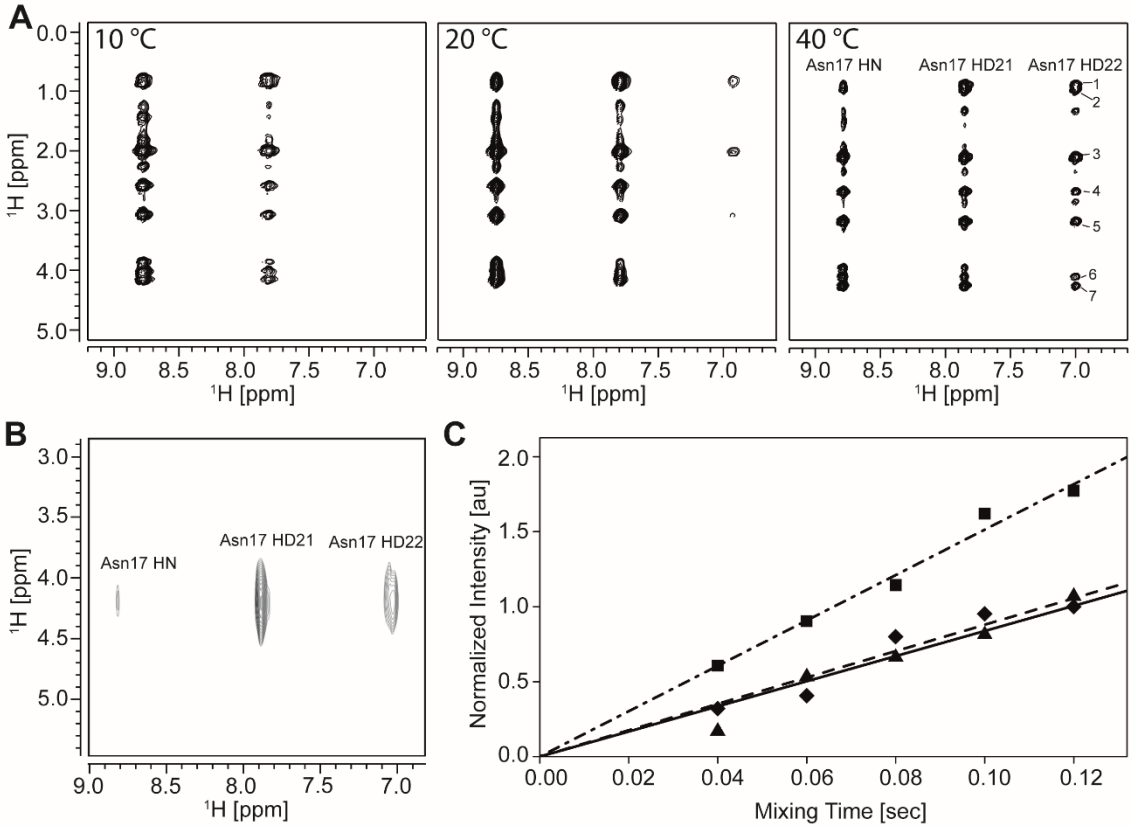

Figure 3. Multi-dimensional NOE experiments to estimates inter-chain side-chain contacts. (**A**) ^{15}N-edited NOESY at 10 °C, 20 °C, and 40 °C. Assignments: 1 = HD1 Leu13/Leu20, 2 = HD2 Leu13/Leu20, 3 = βH Leu13/Leu20, 4/5 = βH Asn17, 6 = αH Leu13, 7 = αH Asn17/Leu20. (**B**) 2D plane of the ^{13}C-HSQC-NOESY-^{15}N-HMQC showing cross peaks between Asn17 and Leu13 of the partnering peptides. (**C**) Relative intensity plot of Asn17(HN) (rhombus, dashed line), HD21 (square, dashed-dotted line), and HD22 (triangle, solid line) as a function of mixing time in 1D spectra of ^{13}C-HSQC-NOESY-^{15}N-HMQC. Intensities were normalized to Asn17(HN). Conditions: 2 mM total peptide concentration, 10 mM phosphate buffer (68 mM sodium chloride, 1.4 mM potassium chloride, pH adjusted to 7.0), 10% D_2O, using a cryoprobe-equipped Bruker 600 MHz spectrometer (**A,C**) or 800 MHz spectrometer (**B**).

Non-hydrogen-bonding conformations are also populated. At μM concentrations, CC-Di has a midpoint melting temperature of 78 ˚C and its thermal unfolding transition starts above 40 ˚C.[17] This stability allowed us to investigate the temperature dependence of signal broadening, and so to probe side-chain dynamics further, through 3D ^{15}N-edited NOESY at 10 °C, 20 °C and 40 °C for CC-Di$_N$(Asn). In the ^{1}H-^{1}H planes of these spectra, Fig. 3A, peaks became sharper and more resonances appeared for Asn17 as the temperature was raised. By 40 °C all peaks were sharpened and the HD22 resonances were visible. We used this 40 °C spectrum to assign NOE contacts to the Asn side-chain amide protons. The most intensive NOEs were to leucine (Leu) side chains, Leu13 or Leu20, which flank Asn17 in the hydrophobic core. This indicates strongly that the Asn side chains are buried in the hydrophobic core as expected. However, this experiment has a caveat: it does not distinguish intra- and inter-strand NOEs.

To address this, we made a third CC-Di peptide variant, CC-Di$_C$(Leu13), with Leu13 ^{13}C- labelled at the Cα position (Table S1, Fig. S4), and mixed this with CC-Di$_N$(Asn) for 4D NOE experiments (^{13}C-HSQC-NOESY-^{15}N-HMQC).[60] The peptides were mixed 1:1, which, all other things being equal, should have given 50% hetero-labelled dimers. Consistent with this, the (^{1}H, ^{1}H) plane from the 4D experiment revealed NOEs between all three nitrogen-bound protons of Asn17 and the Cα proton of Leu13 (Fig. 3B). This is only possible if the two labelled peptides are complexed and the Asn side chains spend at least some time buried in the interface. Moreover, the NOEs from Leu13 had different intensities: the weakest was to the backbone NH of Asn17, that for the HD22 proton was also weak but slightly more intensive, and the strongest was for HD21. This suggests decreasing contact distances between these pairs of protons, again consistent with at least partial burial of the Asn side chains.

We estimated the Leu13-to-Asn17(HD21/HD22) inter-proton distances relative to that for Leu13-Asn17(HN) through an inter-peptide NOE-build-up experiment with mixing times of 40 ms - 120 ms (Fig. 3C). This gave cross-relaxation rate constants for HN, HD21 and HD22. From the X-ray crystal structure of CC-Di, the Leu13(CαH) to Asn17(NH) distance is 7.5 Å (Fig. S7). As molecular dynamics simulations (*vide infra*) suggested that the backbone structure of the dimer is relatively rigid, we used this as a reference to estimate the other distances Leu13(CαH) to Asn17(HD21/HD22) (Methods and Table S3). In this way, we measured the Leu13(CαH) to Asn17(HD21) and Asn17(HD22) distances both as ≈7 Å, which we recognize are averages over the experimental time. From the X-ray crystal structure and MD simulations of CC-Di, with both Asn side chains buried (*i.e.*, 'inside' or 'middle' conformations) these distances are expected to be 3.3 Å – 6.3 Å (Fig. S7 A–D) and if they adopt out-conformations 6.5 Å – 7.6 Å (Fig. S7 E). That the experimentally determined distances are towards the higher ends of these ranges indicates strongly that the non-hydrogen-bonding out-conformations do exist in solution and with a significant population, together with 'inside'- and 'middle'-conformations. However, since many conformations are potentially present, each with different distances resulting in different NOE enhancements, it is not possible to infer their relative populations.

Asparagine conformers exchange on the millisecond time scale. To probe the dynamics of Asn17 in the dimer, we performed two relaxation NMR experiments with a peptide, CC-Di$_N$(Leu,Asn), in which the four Leu residues at ***d*** positions and Asn17 were fully ^{15}N-labelled (Table S1, Fig. S5).

First, model-free analyses were carried out for backbone-amide protons. These probe fast motions on the ps – ns timescale. This is done by transforming observable relaxation parameters, T1, T2 and hetero-nuclear NOEs (Table S4) into interpretable parameters: the squared generalized order parameter (S^2) and the effective correlation time (τ_e),[48] which indicate the amplitude and the timescale of local motions, respectively. We employed the method of d'Auvergne and Gooley, which refines the model-free coefficients using an independent tumbling time τ_m for each residue and a selection of diffusion models to compute S^2 and τ_e (RELAX).[54] The S^2 values for all of the backbone amide protons were closely similar at ≈ 0.8 (Fig. 4A and Table S5). This revealed that the majority of the backbone structure of the peptide was almost evenly rigid. However, notably, the S^2 value for Asn17 was the largest among 5 labelled residues, indicating that the motion of the Asn17-NH bond was the most restricted. Also, its τ_e was the largest, and by a factor of 2 compared with the neighboring leucines. These experiments and analyses illustrates that Asn17 has unique internal motions compared to the more-rigidly held leucines in the dimer interface.

Second, to investigate conformational exchange of the Asn17 side chain, we performed relaxation-dispersion experiments.[61,62] These detect slow chemical exchange in the µs to ms regime by acquiring a series of *Carr-Purcell-Meiboom-Gill* (CPMG) sequence experiments with varying refocusing pulse delays (Fig. 4C). The data indicated that the Asn17 side-chain conformers exchange in the 10 – 100 ms regime, while none of backbone-amide protons exhibits any comparable exchange (Fig. S8). The exchange rate for HD21 was calculated more precisely at 20 s^{-1} ± 4 s^{-1}. However, due to the broader line shape of HD22, no exchange model could be reasonably fitted. This calculated value likely combines exchanges between several conformers at several exchange times and motion on a shorter time scale. Nonetheless, considering that the results of the NOE experiments indicated that the main Asn17 side-chain conformers were with an out-conformation, it is likely that these will experience an exchange regime in the 10 – 100 ms.

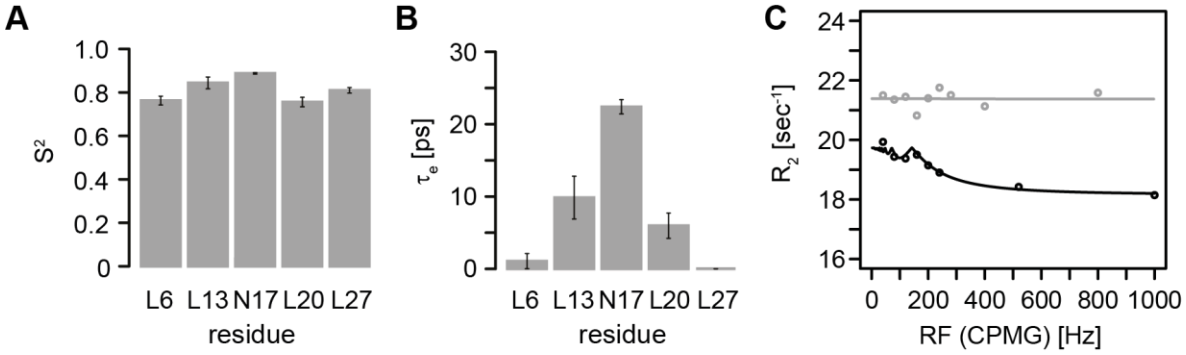

Figure 4. Dynamics in CC-Di investigated by NMR experiments. (**A**) S^2 and (**B**) τ_e values obtained from model-free analyses for backbone amide protons of Leu6, Leu13, Asn17, Leu20 and Leu27. An S^2 of 1.0 indicates the greatest restriction of bond-vector motion. (**C**) Relaxation dispersion curves for Asn17(HD21) at 600 MHz (black) and 700 MHz (gray). The plots were obtained from a series of CPMG sequence experiments with varying refocusing frequencies (RF (CPMG)). The data intensity at each of the refocusing frequencies was converted into an R_2 value and the resulting curve fitted to the Bloch-McConnell equations to extract the exchange rate R_{ex}.[55] The line is the fit of the selected model: "CR72 Full" slow exchange giving a R_{ex} of 20 s^{-1} ± 4 s^{-1}. Conditions: 1 mM total peptide concentration, 10 mM phosphate buffer (68 mM sodium chloride, 1.4 mM potassium chloride, pH adjusted to 7.0), 50% D_2O, using a cryoprobe-equipped Bruker 600 and 700 MHz spectrometer with ^2H decoupling.

Asparagines at a form hydrogen bonds that exchange on ps – ns timeframe. To explore Asn conformations within CC interfaces and to examine how these might influence oligomeric-state selection, we performed Replica-Exchange Molecular Dynamics (REMD) simulations.[62] Starting structures were generated from the X-ray crystal structure of CC-Di.[17] From possible starting conformations for the Asn17 pair (Fig. 1A), we selected that with both Asn side-chain amide groups pointing 'out' towards solvent. We chose this to test if a hydrogen bond would form between the Asn side chains during the simulation, rather than starting with a lower-energy hydrogen-bonded state and attempting to see bond rupture. Indeed, we found that hydrogen bonding between the Asn side chains appeared at ≈ 200 ps into the simulation. This became the default state around 5 ns and the structure remained stable from that point on (Fig. 5A). Nonetheless, the hydrogen bond was very dynamic. The Asn residues switched frequently between two forms of one conformation with concomitant breaking and reforming of the hydrogen bonds (Fig. S9C). The conformation observed matched the most popular hydrogen-bonded conformation from the PDB analysis (Fig. 1 C(i)), *i.e.*, ***g*⁻*o*/*tg*⁻** or 'inside-middle'. What was not obvious from the latter static structures, but became apparent in the REMD, was that the Asn residues interconvert between the two equivalent conformations, ***g*⁻*o*/*tg*⁻** and ***tg*⁻/*g*⁻*o***: effectively, the side chains of the two peptides switch conformations and, therefore, exchange between being a hydrogen-bond acceptor and a donor, (Fig. 5C). This interconversion occurred ~2800 times in ~7800 consecutive snapshots of the simulation that had exactly one hydrogen bond between the two residues; *i.e.*, the hydrogen bond was retained between steps but the conformation of the asparagine pair switched.

Thus, pairs of Asn residues at ***a*** are accommodated in the otherwise hydrophobic interfaces of parallel CC dimers, and some of the loss in solvation energy is compensated by the formation of inter-helix side-chain interactions. However, these hydrogen bonds are not static but extremely dynamic, with different rotamers of the Asn being explored to effect exchange between outward and inward facing amides groups, with only the latter leading to hydrogen bonding.

For comparison, a second REMD simulation was performed with Asn residues at a ***d*** position of CC-Di. For this, a starting structure was constructed from 4DZM in which position 17 was mutated to Ile, to match the other ***a*** positions in the structure, and position 13 was mutated to Asn. Asn rotamers were chosen based on the small number of CC dimers found in CC+ with Asn at ***d***.[16] In contrast to the Asn-at-***a*** simulation, the second calculation revealed that Asn residues paired at ***d*** positions rarely form a hydrogen bond (Fig. 5B). Moreover, on the odd occasion that a hydrogen bond was made it was at the expense of the overall structure: a kink formed in the helix near the Asn position (Fig. S9D); this destabilizes the core; and the helical structure unfolds *C* terminal to the Asn residues. Consistent with this, we found that Asn occurs only rarely at ***d*** positions in dimeric CC structures: there were 19 examples in CC+ at 50% redundancy, compared with 128 examples of Asn at ***a*** sites.[17] Interestingly, the majority of the former also have an Asn at ***a***,

which may help accommodate an Asn at the ***d*** position by specifying the dimer state. These findings are consistent with recently described experimental systems that show that Asn at ***d*** destablizes dimers more than Asn at ***a***, and that Asn at ***d*** is better accommodated in parallel trimeric CCs.[17,24,32]

DISCUSSION

The coiled-coil (CC) motif is one of the most widely used peptide building blocks in synthetic biology and biomaterials.[2,3] Such work relies on having sequence-to-structure relationships to guide and deliver peptide designs *de novo*. Ideally, these relationships should be understood at the physico-chemico level. For CCs such rules do exist, but the underlying mechanisms of action are not understood for all of these. Here we focus on examining in detail one such rule of thumb; namely, that asparagine (Asn) residues placed at the ***a*** sites of the heptad sequences repeats of CCs, ***abcdefg***, directs the formation of parallel dimeric CCs. These positions are traditionally considered as being buried within the otherwise hydrophobic CC interface, and, as such, they are usually paired with another Asn residue in the partnering strand of the CC. It is assumed in the literature that specificity for parallel, in-register dimers in conferred by the abilities of these Asn pairs to form inter-side-chain hydrogen bonds.

Our study combines bioinformatics analysis of known X-ray crystal structures of dimeric CCs to explore the static conformations accessible to these buried Asn residues; and NMR experiments and molecular-dynamics (MD) simulations to probe the dynamic states accessible to these pairings. The CC crystal structures show different conformations for Asn where the side chain points 'inside', towards the 'middle' and 'outside' of the CC interface. Only certain combinations have the potential to make side-chain hydrogen bonds, however; namely, 'inside-middle'. Although other paired conformers are observed, this is by far the dominant one.

2D NMR experiments of a designed CC dimer with an Asn-at-***a*** (CC-Di) confirm a fully α-helical structure, but importantly, reveal significant broadening of both the Asn backbone and side-chain resonances indicative of chemical exchange. Intra- and inter-strand NOE contacts to the Asn residues are obtained from in 3D and 4D NMR experiments with ^{15}N labelled peptides. These confirm contacts to neighboring leucine residues of the hydrophobic core, but show reduced intensity cross peaks indicating that the Asn side chains are not exclusively inside the core. Moreover, many of the possible combinations of 'inside', 'middle' and 'out' conformations appear to be populated in an ensemble of local structures. These dynamics are probed further with model-free analysis and relaxation dispersion. The former confirm that the backbone structure of the CC-Di is evenly rigid, but with unique internal motions for Asn17; and the latter reveal ms chemical exchange of its side-chain amide protons. Together, these data strongly suggest that Asn17 side chain is in conformational exchange on a 10 – 100 ms time scale. MD studies of CC-Di, initiated with non-hydrogen-bonded 'inside-inside' pair conformation, confirm the formation of the 'inside-middle' hydrogen bond, and that this is a highly dynamic state switching between two analogous side-chain dihedral conformations. By contrast, MD simulations of a CC-Di variant with Asn-at-***d*** show that the side chains are unable to form hydrogen-bonded pairs in a parallel CC dimer. This accords with the relatively few examples of CCs with Asn-at-***d***,[16,63-65] and with a recent experimental study in which the Leu13→Asn mutation of CC-Di loses dimer specificity.[32] This underlines the importance and worth of Asn-at-***a*** as a protein-design rule

Taking all of these results into account, we propose the following model (Fig. 5C): Asn residues at the ***a*** positions of parallel coiled-coil dimers increase the

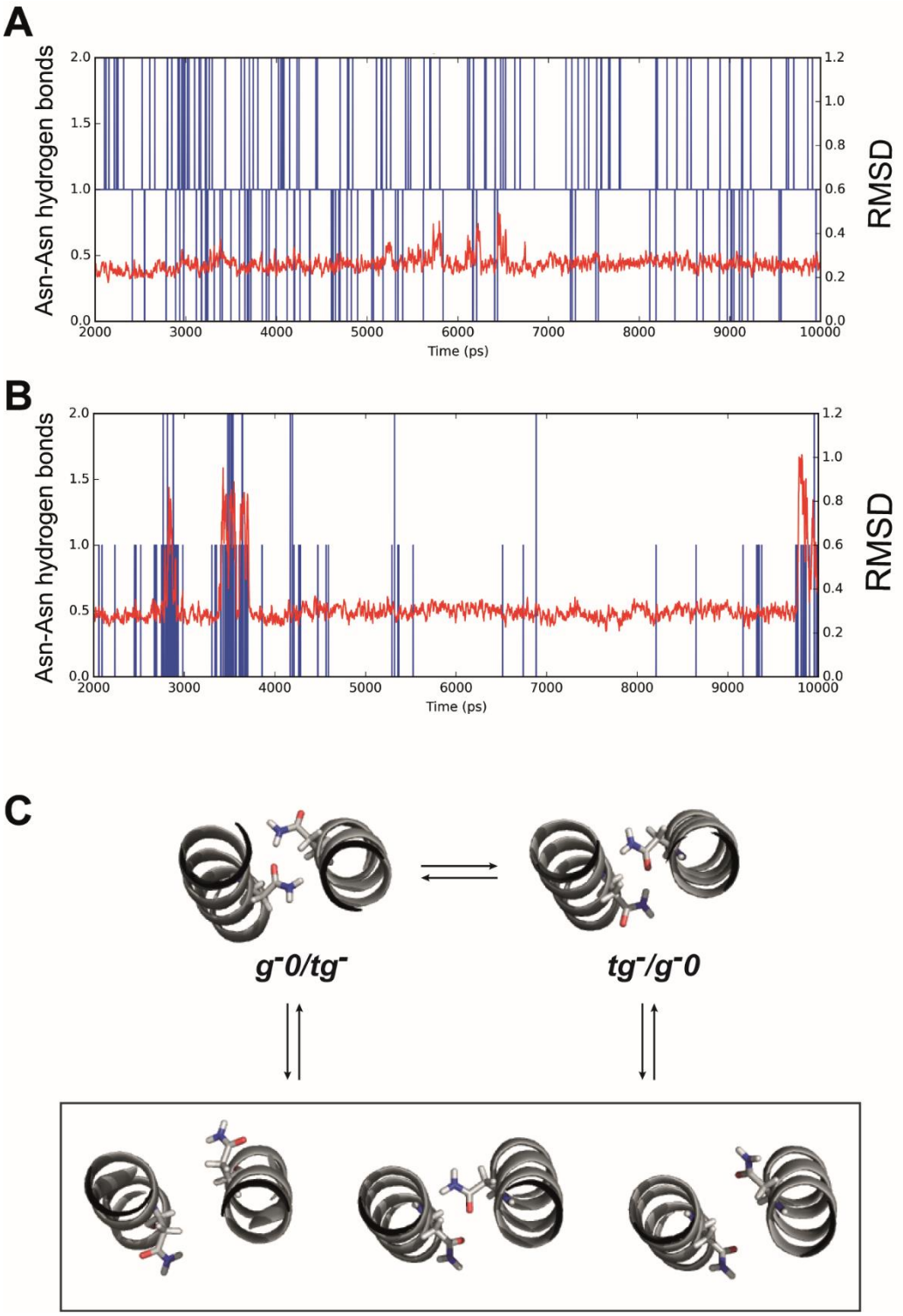

Figure 5. Dynamic equilibria of the Asn side-chain conformations. (**A&B**) The last 8000 ps of the molecular-dynamics (MD) trajectories at 313 K for the Asn-at-***a*** (**A**) and Asn-at-***d*** (**B**) systems described in the text. Full details of the REMD protocol can be found in the SI. The number of hydrogen bonds made between the two Asn residues in the core is shown in blue, and the backbone RMSD in red. The Asn-at-***a*** simulation showed continual interchange between side-chain conformations. By contrast, there were very few hydrogen bonds made between Asn-at-***d***. and where they occurred they were short lived. (**C**) Proposed model of the dynamic processes of the Asn pair in CC-Di.

dimer specificity because the formation of a hydrogen bond between side-chain amide groups is generally enabled. However, the Asn pair can adopt several conformations in a dynamic equilibrium. The most preferred conformations are the two 'inside-middle' pairs, $g^{-}o/tg^{-}$ and $tg^{-}/g^{-}o$. These both lead to hydrogen-bond formation between the Asn side chains, and there is fast exchange between the two conformations. This constant bond breaking and making occasionally results in a switch from an 'inside-middle' conformation to 'out' conformations, most likely driven by the hydrophilicity of the Asn residue. Subsequent hydrogen-bond formation is potentially slowed because the 'out' conformations can be stabilized by contacts to polar groups and water. This chemical exchange in the ms regime is likely to be responsible for signal broadening of the asparagine resonances in the NMR experiments.

Our model has features in common with that from a foregoing study on NMR studies of the Jun leucine zipper, which is another CC dimer.[46] However, we have been able to address details and specifics of the mechanism to an unprecedented level by: identifying the different conformation states that are possible through analyses of many X-ray crystal structures; quantifying the timescales of the dynamics and exchange processes with multi-dimensional NMR experiments; validating a sequential mechanism for these processes using MD simulations; and comparing data for how different Asn inclusions specify dimer or not. This presents a holistic view of the roles of buried Asn residues in promoting and maintaining CC-dimer states.

A recent NMR study by Kaplan *et al.* further highlights the significance of the dynamics of side chains on CC structure.[44] As pH is lowered from near neutral to acidic in the GCN4-p1 system, inter-chain salt-bridges are lost and the titratable (glutamate and lysine) side chains involved become more dynamic. As a consequence, and although helicity and CC interactions are maintained, the whole structure relaxes with the helices moving slightly further apart and the supercoil unwinding slightly.

Whilst these and other studies illustrate that dynamics in CC systems have not been entirely overlooked, it is true to say that much of knowledge of these relationships comes from examining static structures and experiments that assume near-static structures. Our study adds to this move towards a holistic view of these assemblies that considers dynamics as well. We have focused on buried Asn residues in CC dimers and found that these are far more dynamic than previously thought with the inclusion of different Asn conformations in the hydrogen-bonded state, and even that the Asn side chains temporarily shift outside of the hydrophobic core. The latter observation has not been described in any foregoing reports. This helps to explain why the incorporation of polar residues is actually destabilizing, because a favorable contribution from buried polar residues to stability is only possible if the unfavorable energy of dehydration is completely compensated by hydrogen bonding within the folded state.[66-70] Understanding of these effects should help in the design of alternative specification motifs for distinguishing between CC states. Indeed, this has been attempted to some extent, though without considerations of structural dynamics, using urea and guanidinium recognition motifs.[71-73] Generally, incorporating dynamical aspects of CC structure, assembly and specificity will improve our ability to model, engineer and design these important protein-protein recognition motifs.

ASSOCIATED CONTENT

The supporting information contains materials and methods as well as additional figures and tables.

AUTHOR INFORMATION

Corresponding Author

* fthomas@gwdg.de, D.N.Woolfson@bristol.ac.uk

Author Contributions

FT, AN and DNW designed experiments. FT and AN synthesized the peptides. FT, AN and AO recorded and analyzed the NMR spectra. GJB performed the analyses of the Protein Data Bank and MD simulations. All authors contributed to writing the manuscript. ‡These authors contributed equally.

ACKNOWLEDGMENT

FT and DNW are grateful for financial support from the Leverhulme Trust (RPG-2012-536). AN and DNW were funded by the BBSRC (BB/J009784/1). AN, GJB and DNW were funded by the ERC (340764). DNW holds a Royal Society Research Merit Award (WM140008). We appreciate the support of the MRC Biomedical NMR Centre at the Francis Crick Institute, London, which is core funded by Cancer Research UK, the UK Medical Research Council, and the Wellcome Trust (FC001142, FC10029). We thank Tom Frenkiel, Geoff Kelly, Matt Crump, Craig Butts, Emily Baker and Richard Sessions for fruitful discussions.

REFERENCES

[1] Lupas, A. N., and Bassler, J. (2017) Coiled Coils - A Model System for the 21st Century, *Trends Biochem. Sci. 42*, 130-140.

[2] Woolfson, D. N. (2017) Coiled-Coil Design: Updated and Upgraded, *Sub-Cellular Biochemistry 82*, 35-61.

[3] Boyle, A. L., and Woolfson, D. N. (2011) De novo designed peptides for biological applications, *Chem. Soc. Rev. 40*, 4295-4306.

[4] Marsden, H. R., and Kros, A. (2010) Self-Assembly of Coiled Coils in Synthetic Biology: Inspiration and Progress, *Angew. Chem. Int. Ed. 49*, 2988-3005.

[5] Woolfson, D. N., Bartlett, G. J., Bruning, M., and Thomson, A. R. (2012) New currency for old rope: from coiled-coil assemblies to alpha-helical barrels, *Current Opinion in Structural Biology 22*, 432-441.

[6] Crick, F. H. C. (1953) The packing of alpha-helices - simple coiled-coils, *Acta Crystallographica 6*, 689-697.

[7] Thomson, A. R., Wood, C. W., Burton, A. J., Bartlett, G. J., Sessions, R. B., Brady, R. L., and Woolfson, D. N. (2014) Computational design of water-soluble alpha-helical barrels, *Science 346*, 485-488.

[8] Harbury, P. B., Zhang, T., Kim, P. S., and Alber, T. (1993) A switch between 2-stranded, 3-stranded and 4-stranded coiled coils in GCN4 leucine-zipper mutants, *Science 262*, 1401-1407.

[9] O'Shea, E. K., Lumb, K. J., and Kim, P. S. (1993) Peptide Velcro - Design of a heterodimeric coiled-coil, *Curr. Biol. 3*, 658-667.

[10] McClain, D. L., Gurnon, D. G., and Oakley, M. G. (2002) Importance of potential interhelical salt-bridges involving interior residues for coiled-coil stability and quaternary structure, *J. Mol. Biol. 324*, 257-270.

[11] Steinmetz, M. O., Jelesarov, I., Matousek, W. M., Honnappa, S., Jahnke, W., Missimer, J. H., Frank, S., Alexandrescu, A. T., and Kammerer, R. A. (2007) Molecular basis of coiled-coil formation, *Proc. Natl. Acad. Sci. U.S.A. 104*, 7062-7067.

[12] Litowski, J. R., and Hodges, R. S. (2002) Designing heterodimeric two-stranded alpha-helical coiled-coils - Effects of hydrophobicity and alpha-helical propensity on protein folding, stability, and specificity, *J. Biol. Chem. 277*, 37272-37279.

[13] Thomas, F., Boyle, A. L., Burton, A. J., and Woolfson, D. N. (2013) A Set of de Novo Designed Parallel Heterodimeric Coiled Coils with Quantified Dissociation Constants in the Micromolar to Sub-nanomolar Regime, *J. Am. Chem. Soc. 135*, 5161-5166.

[14] Monera, O. D., Kay, C. M., and Hodges, R. S. (1994) Electrostatic interactions control the parallel and antiparallel orientation of alpha-helical chains in two-stranded alpha-helical coiled-coils, *Biochemistry 33*, 3862-3871.

[15] Berman, H. M., Westbrook, J., Feng, Z., Gilliland, G., Bhat, T. N., Weissig, H., Shindyalov, I. N., and Bourne, P. E. (2000) The Protein Data Bank, *Nucleic Acids Res. 28*, 235-242.

[16] Testa, O. D., Moutevelis, E., and Woolfson, D. N. (2009) CC plus : a relational database of coiled-coil structures, *Nucleic Acids Res. 37*, D315-D322.

[17] Fletcher, J. M., Boyle, A. L., Bruning, M., Bartlett, G. J., Vincent, T. L., Zaccai, N. R., Armstrong, C. T., Bromley, E. H. C., Booth, P. J., Brady, R. L., Thomson, A. R., and Woolfson, D. N. (2012) A basis set of de novo coiled-coil peptide oligomers for rational protein design and synthetic biology, *ACS Synth. Biol. 1*, 240-250.

[18] Zeng, X., Herndon, A. M., and Hu, J. C. (1997) Buried asparagines determine the dimerization specificities of leucine zipper mutants, *Proc. Natl. Acad. Sci. U.S.A. 94*, 3673-3678.

[19] Zhu, H., Celinski, S. A., Scholtz, J. M., and Hu, J. C. (2000) The contribution of buried polar groups to the conformational stability of the GCN4 coiled coil, *J. Mol. Biol. 300*, 1377-1387.

[20] Oakley, M. G., and Kim, P. S. (1998) A buried polar interaction can direct the relative orientation of helices in a coiled coil, *Biochemistry 37*, 12603-12610.

[21] Akey, D. L., Malashkevich, V. N., and Kim, P. S. (2001) Buried polar residues in coiled-coil interfaces, *Biochemistry 40*, 6352-6360.

[22] Rackham, O. J. L., Madera, M., Armstrong, C. T., Vincent, T. L., Woolfson, D. N., and Gough, J. (2010) The Evolution and Structure Prediction of Coiled Coils across All Genomes, *J. Mol. Biol. 403*, 480-493.

[23] Eckert, D. M., Malashkevich, V. N., and Kim, P. S. (1998) Crystal structure of GCN4-pIQI, a trimeric coiled coil with buried polar residues, *J. Mol. Biol. 284*, 859-865.

[24] Hartmann, M. D., Ridderbusch, O., Zeth, K., Albrecht, R., Testa, O., Woolfson, D. N., Sauer, G., Dunin-Horkawicz, S., Lupas, A. N., and Alvarez, B. H. (2009) A coiled-coil motif that sequesters ions to the hydrophobic core, *Proc. Natl. Acad. Sci. U.S.A. 106*, 16950-16955.

[25] O'Shea, E. K., Klemm, J. D., Kim, P. S., and Alber, T. (1991) X-ray structure of the GCN4 leucine zipper, a 2-stranded, parallel coiled coil, *Science 254*, 539-544.

[26] Glover, J. N. M., and Harrison, S. C. (1995) Crystal-structure of the heterodimeric bzip transcription factor c-Fos-c-Jun bound to DNA, *Nature 373*, 257-261.

[27] Lumb, K. J., and Kim, P. S. (1995) A buried polar interaction imparts structural uniqueness in a designed heterodimeric coiled coil, *Biochemistry 34*, 8642-8648.

[28] Gonzalez, L., Woolfson, D. N., and Alber, T. (1996) Buried polar residues and structural specificity in the GCN4 leucine zipper, *Nat. Chem. Biol. 3*, 1011-1018.

[29] Gradisar, H., and Jerala, R. (2011) De novo design of orthogonal peptide pairs forming parallel coiled-coil heterodimers, *J Pept Sci 17*, 100-106.

[30] Crooks, R. O., Lathbridge, A., Panek, A. S., and Mason, J. M. (2017) Computational Prediction and Design for Creating Iteratively Larger Heterospecific Coiled Coil Sets, *Biochemistry 56*, 1573-1584.

[31] Drobnak, I., Gradisar, H., Ljubetic, A., Merljak, E., and Jerala, R. (2017) Modulation of Coiled-Coil Dimer Stability through Surface Residues while Preserving Pairing Specificity, *J. Am. Chem. Soc. 139*, 8229-8236.

[32] Fletcher, J. M., Bartlett, G. J., Boyle, A. L., Danon, J. J., Rush, L. E., Lupas, A. N., and Woolfson, D. N. (2017) N@a and N@d: Oligomer and partner specification by asparagine in coiled-coil interfaces, *ACS Chem. Biol. 12*, 528-538.

[33] Wu, Y. Y., and Collier, J. H. (2017) alpha-Helical coiled-coil peptide materials for biomedical applications, *Wiley Interdiscip. Rev. Nanomed. Nanobiotechnol. 9*, e1424.

[34] Boyle, A. L., Bromley, E. H. C., Bartlett, G. J., Sessions, R. B., Sharp, T. H., Williams, C. L., Curmi, P. M. G., Forde, N. R., Linke, H., and Woolfson, D. N. (2012) Squaring the Circle in Peptide Assembly: From Fibers to Discrete Nanostructures by de Novo Design, *J. Am. Chem. Soc. 134*, 15457-15467.

[35] Gradisar, H., Bozic, S., Doles, T., Vengust, D., Hafner-Bratkovic, I., Mertelj, A., Webb, B., Sali, A., Klavzar, S., and Jerala, R. (2013) Design of a single-chain polypeptide tetrahedron assembled from coiled-coil segments, *Nat Chem Biol 9*, 362-366.

[36] Boyken, S. E., Chen, Z. B., Groves, B., Langan, R. A., Oberdorfer, G., Ford, A., Gilmore, J. M., Xu, C. F., DiMaio, F., Pereira, J. H., Sankaran, B., Seelig, G., Zwart, P. H., and Baker, D. (2016) De novo design of protein homo-oligomers with modular hydrogen-bond network-mediated specificity, *Science 352*, 680-687.

[37] Lavigne, P., Sonnichsen, F. D., Kay, C. M., and Hodges, R. S. (1996) Interhelical salt bridges, coiled-coil stability, and specificity of dimerization, *Science 271*, 1136-1137.

[38] Lumb, K. J., and Kim, P. S. (1996) Interhelical salt bridges, coiled-coil stability, and specificity of dimerization - Response, *Science 271*, 1137-1138.

[39] Meier, M., Stetefeld, J., and Burkhard, P. (2010) The many types of interhelical ionic interactions in coiled coils - An overview, *J. Struct. Biol. 170*, 192-201.

[40] Marti, D. N., and Bosshard, H. R. (2004) Inverse electrostatic effect: Electrostatic repulsion in the unfolded state stabilizes a leucine zipper, *Biochemistry 43*, 12436-12447.

[41] Marti, D. N., and Bosshard, H. R. (2003) Electrostatic interactions in leucine zippers: Thermodynamic analysis of the contributions of Glu and his residues and the effect of mutating salt bridges, *J. Mol. Biol. 330*, 621-637.

[42] Lumb, K. J., and Kim, P. S. (1995) Measurement of interhelical electrostatic interactions in the GCN4 leucine-zipper, *Science 268*, 436-439.

[43] Matousek, W. M., Ciani, B., Fitch, C. A., Garcia-Moreno, B., Kammerer, R. A., and Alexandrescu, A. T. (2007) Electrostatic contributions to the stability of the GCN4 leucine zipper structure, *J. Mol. Biol. 374*, 206-219.

[44] Kaplan, A. R., Brady, M. R., Maciejewski, M. W., Kammerer, R. A., and Alexandrescu, A. T. (2017) Nuclear Magnetic Resonance Structures of GCN4p Are Largely Conserved When Ion Pairs Are Disrupted at Acidic pH but Show a Relaxation of the Coiled Coil Superhelix, *Biochemistry 56*, 1604-1619.

[45] Oshaben, K. M., Salari, R., McCaslin, D. R., Chong, L. T., and Horne, W. S. (2012) The Native GCN4 Leucine-Zipper Domain Does Not Uniquely Specify a Dimeric Oligomerization State, *Biochemistry 51*, 9581-9591.

[46] Junius, F. K., Mackay, J. P., Bubb, W. A., Jensen, S. A., Weiss, A. S., and King, G. F. (1995) Nuclear-magnetic-resonance characterization of the Jun leucine-zipper domain - unusual properties of coiled-coil interfacial polar residues, *Biochemistry 34*, 6164-6174.

[47] Schanda, P., and Brutscher, B. (2005) Very Fast Two-Dimensional NMR Spectroscopy for Real-Time Investigation of Dynamic Events in Proteins on the Time Scale of Seconds, *J. Am. Chem. Soc. 127*, 8014-8015.

[48] Lipari, G., and Szabo, A. (1982) Model-free approach to the interpretation of nuclear magnetic-resonance relaxation in macromolecules. 1. Theory and range of validity, *J. Am. Chem. Soc. 104*, 4546-4559.

[49] Mulder, F. A. A., Skrynnikov, N. R., Hon, B., Dahlquist, F. W., and Kay, L. E. (2001) Measurement of slow (mu s-ms) time scale dynamics in protein side chains by N-15 relaxation dispersion NMR spectroscopy: Application to Asn and Gln residues in a cavity mutant of T4 lysozyme, *J. Am. Chem. Soc. 123*, 967-975.

[50] Zuiderweg, E. R. P., Petros, A. M., Fesik, S. W., and Olejniczak, E. T. (1991) 4-Dimensional C-13, H-1, C-13, H-1 HMQC-NOE-HMQC NMR-spectroscopy - resolving tertiary NOE distance constraints in the spectra of larger proteins., *J. Am. Chem. Soc. 113*, 370-372.

[51] Vögeli, B. (2014) The nuclear Overhauser effect from a quantitative perspective, *Prog. Nucl. Magn. Reson. Spectrosc. 78*, 1-46.

[52] Neuhaus, D., and Williamson, M. P. (1989) *The Nuclear Overhauser Effect in Structural and Conformational Analysis*, 2 ed., Wiley-VHC.

[53] Delaglio, F., Grzesiek, S., Vuister, G. W., Zhu, G., Pfeifer, J., and Bax, A. (1995) NMRPipe - a multidimensional spectral processing system based on unix pipes, *J. Biomol. NMR 6*, 277-293.

[54] d'Auvergne, E. J., and Gooley, P. R. (2008) Optimisation of NMR dynamic models II. A new methodology for the dual optimisation of the model-free parameters and the Brownian rotational diffusion tensor, *J. Biomol. NMR 40*, 121-133.

[55] BlueCrystal:, http://www.acrc.bris.ac.uk/.

[56] Lovell, S. C., Word, J. M., Richardson, J. S., and Richardson, D. C. (1999) Asparagine and glutamine rotamers: B-factor cutoff and correction of amide flips yield distinct clustering, *Proc. Natl. Acad. Sci. U.S.A. 96*, 400-405.

[57] McLachlan, A. D. (1982) Rapid comparison of protein structures, *Acta Crystallogr. Sect. A 38*, 871-873.

[58] Wang, T., Darwin, K. H., and Li, H. L. (2010) Binding-induced folding of prokaryotic ubiquitin-like protein on the Mycobacterium proteasomal ATPase targets substrates for degradation, *Nat. Struct. Mol. Biol. 17*, 1352-U1208.

[59] Kjaergaard, M., and Poulsen, F. M. (2011) Sequence correction of random coil chemical shifts: correlation between neighbor correction factors and changes in the Ramachandran distribution, *J. Biomol. NMR 50*, 157-165.

[60] Kay, L. E., Clore, G. M., Bax, A., and Gronenborn, A. M. (1990) 4-Dimensional heteronuclear triple-resonance NMR-spectroscopy of Interleukin-1-beta in solution, *Science 249*, 411-414.

[61] Liu, A. Z., Yao, L. S., Li, Y., and Yan, H. G. (2007) TROSY of side-chain amides in large proteins, *J Magn Reson 186*, 319-326.

[62] Loria, J. P., Rance, M., and Palmer, A. G. (1999) A relaxation-compensated Carr-Purcell-Meiboom-Gill sequence for characterizing chemical exchange by NMR spectroscopy, *J. Am. Chem. Soc. 121*, 2331-2332.

[63] Murphy, G. A., Spedale, E. J., Powell, S. T., Pillus, L., Schultz, S. C., and Chen, L. (2003) The Sir4 C-terminal coiled coil is required for telomeric and mating type silencing in Saccharomyces cerevisiae, *J. Mol. Biol. 334*, 769-780.

[64] Frye, J., Klenchin, V. A., and Rayment, I. (2010) Structure of the tropomyosin overlap complex from chicken smooth muscle: insight into the diversity of N-terminal recognition, *Biochemistry 49*, 4908-4920.

[65] Qiao, R., Cabral, G., Lettman, M. M., Dammermann, A., and Dong, G. (2012) SAS-6 coiled-coil structure and interaction with SAS-5 suggest a regulatory mechanism in C. elegans centriole assembly, *EMBO J. 31*, 4334-4347.

[66] Kondratova, M. S., and Efimov, A. V. (2002) A systematic analysis of buried polar side chains and their interactions in alpha-helical proteins, *Mol. Biol. 36*, 117-123.

[67] Brazhnikov, E. V., and Efimov, A. V. (2005) Analysis of interactions of buried polar side chains in beta-proteins, *Mol. Biol. 39*, 878-886.

[68] Pace, C. N. (2001) Polar group burial contributes more to protein stability than nonpolar group burial, *Biochemistry 40*, 310-313.

[69] Takano, K., Yamagata, Y., and Yutani, K. (2001) Contribution of polar groups in the interior of a protein to the conformational stability, *Biochemistry 40*, 4853-4858.

[70] Loladze, V. V., Ermolenko, D. N., and Makhatadze, G. I. (2002) Thermodynamic consequences of burial of polar and non-polar amino acid residues in the protein interior, *J. Mol. Biol. 320*, 343-357.

[71] Diss, M. L., and Kennan, A. J. (2008) Orthogonal recognition in dimeric coiled coils via buried polar-group modulation, *J. Am. Chem. Soc. 130*, 1321-1327.

[72] Diss, M. L., and Kennan, A. J. (2008) Heterotrimeric Coiled Coils with Core Residue Urea Side Chains, *J. Org. Chem. 73*, 9752-9755.

[73] Diss, M. L., Kennan, A. J., Diss, M. L., and Kennan, A. J. (2008) Simultaneous Directed Assembly of Three Distinct Heterodimeric Coiled Coils, *Org. Lett.*, 3797-3800.

TOC content